

Spatial Mapping of Lipids at Cellular Resolution in Embryos of Cotton

Patrick J. Horn,^a Andrew R. Korte,^b Purnima B. Neogi,^a Ebony Love,^a Johannes Fuchs,^c Kerstin Strupat,^d Ljudmilla Borisjuk,^c Vladimir Shulaev,^a Young-Jin Lee,^b and Kent D. Chapman^{a,1}

^aDepartment of Biological Sciences, Center for Plant Lipid Research, University of North Texas, Denton, Texas 76203

^bDepartment of Chemistry, Iowa State University and Ames Laboratory–U.S. Department of Energy, Ames, Iowa 50011

^cLeibniz Institute of Plant Genetics and Crop Research, D-06466 Gatersleben, Germany

^dThermo Fisher Scientific, 28199 Bremen, Germany

Advances in mass spectrometry (MS) have made comprehensive lipidomics analysis of complex tissues relatively commonplace. These compositional analyses, although able to resolve hundreds of molecular species of lipids in single extracts, lose the original cellular context from which these lipids are derived. Recently, high-resolution MS of individual lipid droplets from seed tissues indicated organelle-to-organelle variation in lipid composition, suggesting that heterogeneity of lipid distributions at the cellular level may be prevalent. Here, we employed matrix-assisted laser desorption/ionization–MS imaging (MALDI-MSI) approaches to visualize lipid species directly in seed tissues of upland cotton (*Gossypium hirsutum*). MS imaging of cryosections of mature cotton embryos revealed a distinct, heterogeneous distribution of molecular species of triacylglycerols and phosphatidylcholines, the major storage and membrane lipid classes in cotton embryos. Other lipids were imaged, including phosphatidylethanolamines, phosphatidic acids, sterols, and gossypol, indicating the broad range of metabolites and applications for this chemical visualization approach. We conclude that comprehensive lipidomics images generated by MALDI-MSI report accurate, relative amounts of lipid species in plant tissues and reveal previously unseen differences in spatial distributions providing for a new level of understanding in cellular biochemistry.

INTRODUCTION

Technical advances in mass spectrometry (MS) over the past decade have produced a wealth of information on the abundance and identification of metabolites (lipids, carbohydrates, etc.) and proteins in a manner analogous to the implementation of sequencing and microarray tools for genetic applications. This has led to development of new “-omics” techniques (e.g., metabolomics, proteomics, lipidomics, etc.) that focus on analyzing complex chemical compositional data for biological interpretation (Schmelzer et al., 2007; Welti et al., 2007). Until recently, conventional methods for analyzing metabolites by MS involved time-consuming, chemical-based tissue extractions followed by physical/chemical purification (e.g., liquid chromatography) and infusion of samples into the MS (Han and Gross, 2005). While this approach has been valuable for compound identification and quantification, this methodology is limited in its ability to distinguish where these molecules were localized in situ. On the other hand, optical imaging techniques, such as confocal or electron microscopy using selected fluores-

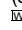
cent dyes, antibodies, and chemical modifications, can hint at cellular localization (Eggeling et al., 2009; Wessels et al., 2010) but currently cannot derive comprehensive compositional information within these images alone.

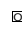
The development of MS imaging (MSI) allows the capability to capture the chemical composition within the spatial context of biological tissues (Cornett et al., 2007; Lee et al., 2012). One type of MSI that offers ease of sample preparation, soft ionization, and MS-based analysis of cellular metabolites is matrix-assisted laser desorption/ionization–MS (MALDI-MS). Improvements in the spatial resolution of MALDI-MSI have progressed from resolutions >200 μm down to submicron levels in some applications (Koestler et al., 2008), with 10 to 50 μm the most commonly achievable spatial resolution at this time. New generations of mass spectrometers capable of extremely high mass resolution and accuracy (Hu et al., 2005; Schaub et al., 2008) make metabolite identification possible at the tissue and cellular levels.

Lipid analysis is particularly amenable to MALDI-MSI. Most of the applications of MALDI-MSI analysis in situ (Murphy et al., 2009; Fuchs et al., 2010) have centered on membrane lipids in mammalian tissues, such as kidney (Murphy et al., 2009), lung (Berry et al., 2011), brain slices in mice (Chen et al., 2008), and whole body imaging (Chaurand et al., 2011). These studies were directed toward spatial analysis of lipid metabolites and have improved our understanding of diseases and genetic mutations. Phospholipids and triacylglycerols (TAGs) imaged in kidney

¹ Address correspondence to chapman@unt.edu.

The author responsible for distribution of materials integral to the findings presented in this article in accordance with the policy described in the Instructions for Authors (www.plantcell.org) is: Kent D. Chapman (chapman@unt.edu).

 Online version contains Web-only data.

 Open Access articles can be viewed online without a subscription. www.plantcell.org/cgi/doi/10.1105/tpc.111.094581

slices show complex molecular distribution profiles that likely result from tightly regulated lipid metabolism (Murphy et al., 2009). Furthermore, a recent article detailing an abundance of phospholipids with polyunsaturated fatty acids (FAs) in the airways of lung tissue by MALDI-MSI demonstrated how spatial organization improves our understanding of how these lipids might be involved in inflammatory responses (Berry et al., 2011). Elsewhere, molecular species of gangliosides in brain slices demonstrated the utility of MALDI-MSI as a histological tool for analyzing models of Tay-Sachs and Sandhoff disease (Chen et al., 2008).

Few examples of MALDI-MSI in situ analysis of plant lipids are available, although several other types of metabolites have been profiled (for a recent review, see Kaspar et al., 2011; Lee et al., 2012). Several studies have adapted MALDI time-of-flight MS to analyze plant lipid extracts, including TAGs from fruit of olives (*Olea europaea*) and pomegranate (*Punica granatum*) seeds (Wiesman and Chapagain, 2009), phosphatidylcholines (PCs) from soybean (*Glycine max*; Zabrouskov et al., 2001), and lipid-soluble pigments (Cai et al., 2006; Suzuki et al., 2009) and galactolipids in plant-like green alga (Vieler et al., 2007). In plant tissues, surface lipids have been mapped in situ on *Arabidopsis thaliana* floral and leaf tissues by MALDI-MSI (Cha et al., 2008; Jun et al., 2010; Vrkoslav et al., 2010). Free FAs were profiled from apple (*Malus domestica*) core and strawberry (*Fragaria* spp) seeds using colloidal graphite as the matrix (Zhang et al., 2007). More recently, imaging MS has been applied to rice grain (*Oryza sativa*) for the analysis of individual PC species (Zaima et al., 2010). Elucidating the spatial distribution of lipid metabolites within plant tissues provides a new perspective to metabolism. This will aid in understanding metabolic compartmentation within plant tissues, help to predict enzyme localization, and provide insights into lipid signaling pathways (Burrell et al., 2007).

Here, we present results of MALDI-MSI approaches to study the distribution of lipids in cotton (*Gossypium hirsutum*) seeds. Cotton is a typical oilseed, storing lipids and proteins in cytosolic organelles of mature seed tissues. In cottonseeds, the amount of stored lipid is ~20% of the seed dry weight (Horn et al., 2011b), making refined cottonseed oil a valuable coproduct of fiber production. However, the antinutritional secondary metabolite, gossypol, must be removed from seed oil extracts through the refining process, and gossypol residues in the protein meal limit its use as a high-value animal feed (Jones and King, 1996). Successful efforts to reduce gossypol levels through genetic engineering approaches are likely to support more widespread use of cottonseed products globally (Sunilkumar et al., 2006). Cottonseed oil is extracted and refined for food applications, and it is composed almost exclusively of TAGs containing linoleic (L; 18:2 at 55 mol %), palmitic (P; 16:0 at 26 mol %), oleic (O; 18:1 at 15 mol %), and stearic (S; 18:0 at 2 mol %) acids (Jones and King, 1996). Several cyclic FAs also are found in TAGs in cottonseeds in minor quantities, including sterculic (Sc; 19:1), dihydrosterculic (Dsc; 19:0), and malvalic acids (Schmid and Patterson, 1988; Obert et al., 2007). Together, these TAG storage molecules are packaged within the seed tissues into lipid droplets surrounded by a single monolayer of polar lipids (e.g., PC).

While the abundance and composition of the lipid molecules in cottonseeds are well defined from chemical extracts (Lísa and Holcapek, 2008; Horn et al., 2011a), there is little information

available about their overall cellular distribution and heterogeneity. Recently, high-resolution MS of individual lipid droplets isolated from cottonseed tissues indicated a marked difference in organelle-to-organelle lipid compositions (Horn et al., 2011a), suggesting that heterogeneity of lipid distributions at the cellular and tissue levels may be prevalent. Our overall objective is to map the chemical distribution of the major and minor storage and membrane lipids throughout the mature cotton embryo tissues and assess the potential heterogeneity of distribution of these molecules by MALDI-MSI. These studies will form the basis for improved spatial understanding of the biosynthetic pathways leading to TAGs in cotton embryos and may suggest potential tissue-specific considerations for the metabolic engineering of oilseeds in general. Further, this approach provides a new tool for the prediction and analysis of lipid metabolism and function in plant tissues more broadly.

RESULTS

General Distribution of Selected Lipid Classes in Cotton Embryos

The reasonably large seed size and the recent MS information on lipid droplet variation (Horn et al., 2011a) made cottonseed a good candidate for analyzing lipid heterogeneity by MALDI-MSI (Figure 1). Total ion intensity profiles were imaged in mature embryos for major storage (TAG) and membrane (PC) lipid classes and compared with summed ion counts for phosphatidylethanolamine (PE), phosphatidic acid (PA), β -sitosterol, and the cotton-specific polyphenolic gossypol (Figure 2). Cross and longitudinal sections were prepared from representative areas of mature cotton embryos (Figure 1), and a raster step size of 50 μm with a laser spot size of ~35 μm was used to sample each section, a resolution about the size of mature cotyledon cells (Chapman et al., 2008). MALDI-MSI profiles (Figure 1D) showed multiple adducts for lipid species (primarily H^+ , Na^+ , and K^+), some substantial ion suppression of TAGs by PC (Emerson et al., 2010), and evidence of diacylglycerol fragments produced by laser-induced compound fragmentation of PC and TAG (Gidden et al., 2007). The molecular species within each lipid class were identified using predefined databases from conventional electrospray ionization-MS (ESI-MS) profiles as well as accurate mass-to-charge ratio (m/z) searches for unique or less prevalent compounds and summed to show distributions for the total classes.

The total ion counts (TICs) for total TAG, PA, and PE were distributed relatively heterogeneously throughout cross and longitudinal sections of embryos (Figures 2B, 2D, and 2E), whereas the total PC ions were more uniformly distributed throughout the cotyledonary tissues, although relatively less abundant within the embryonic axis region of the embryos (Figure 2C). The predominant free sterol in cottonseed tissues, β -sitosterol (Verleyen et al., 2002) (Figure 2F, m/z 397.383 [$\text{M} - \text{H}_2\text{O} + \text{H}$] $^+$), was localized mostly to the embryonic axis. Due to ion suppression of TAG (and other lipids) by PC, there appeared to be relatively more masking of TAG in the cotyledonary tissues, even though there is generally more oil in the cotyledon tissues than in the embryonic axis (Figure 3). This apparent shortcoming of MSI is

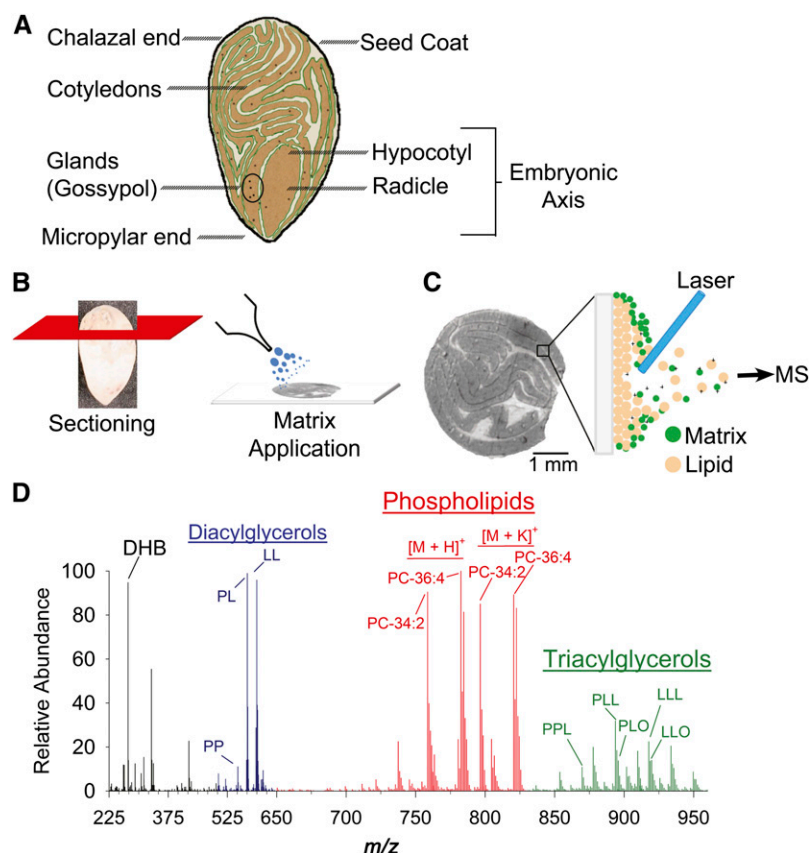


Figure 1. Schematic Overview of Cottonseed Anatomy and the MALDI-MSI Process.

(A) Longitudinal diagram of a mature cotton embryo primarily composed of folded cotyledon tissues surrounding the embryonic axis (hypocotyl and radicle). Pigment glands containing the terpenoid gossypol are present throughout the tissue.

(B) Intact embryos are chemically fixed and sliced into thin cross or longitudinal sections with a cryostat. Sections of $\sim 30 \mu\text{m}$ are adhered to a glass slide and coated with matrix, 2,5-dihydroxybenzoic acid (DHB).

(C) A laser beam is rastered across the section in a serpentine pattern ionizing the seed lipid/matrix mixture at an imaging resolution of $50 \mu\text{m}$. Generated lipid ions as $[M + H]^+$, $[M + Na]^+$, or $[M + K]^+$ adducts are directed into a mass analyzer for the mass spectral data acquisition.

(D) Each laser shot and detection cycle generates a raw data spectrum for each x, y position of the seed section. A sample spectrum shows the identification of the matrix (DHB identified as $[2\text{DHB} - 2\text{H}_2\text{O} + H]^+$ at m/z 273.04) and three distinct compound regions, phospholipids, and in particular PC (red region), TAGs (green region), and diacylglycerols (blue region) from in-source fragmentation of TAG and PC species. Representative species and adducts are labeled with their total acyl composition. For a more comprehensive list of species and adducts identified, see Supplemental Tables 1 to 4 online.

overcome easily by examining mol % distributions within lipid classes (below), but it is important to be cautious not to interpret absolute ion counts as quantitative when comparing lipids across classes. However, relative quantification within lipid classes by MALDI-MSI was remarkably consistent when compared with other methods (see below). Supplemental Figure 1 online shows an example of a raw MS data set and its conversion to a set of MS images for distribution analysis.

The terpenoid gossypol (Figure 2G) is found in the small pigment glands of cottonseed (Adams et al., 1960) and is synthesized for insect and pathogen defense (Hedin et al., 1992; Stipanovic et al., 1999). Gossypol (m/z 501.191) was easily identified in cottonseed sections as a minus-water, protonated species $[M - \text{H}_2\text{O} + H]^+$ and was localized in discrete circular regions in the sections corresponding to the locations of the

pigmented glands. This emphasizes the value of MSI to combine visual structural features with direct chemical information and demonstrates its utility to the localization of plant secondary metabolites.

To compare the distribution of total TAG in embryos by a nondestructive means, intact cottonseeds were subjected to magnetic resonance imaging by $^1\text{H-NMR}$ (Neuberger et al., 2008). Based on NMR imaging of intact seeds (Figure 3; see Supplemental Movie 1 online), there were localized areas enriched in TAG with clear evidence of heterogeneity of total lipid content. There appeared to be regions within cotyledons and within the axis concentrated with more TAG, and not just a uniform, consistent distribution of storage lipid throughout the seed as might be expected. This heterogeneity could be a result of differences in localized enzyme activities or tissue maturity

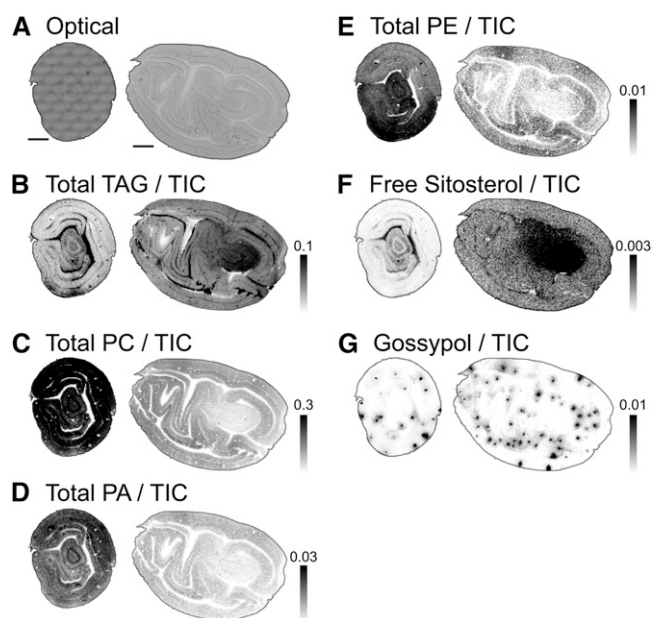


Figure 2. Distribution of Absolute TICs/Intensities of Cottonseed Metabolites.

(A) Optical cross (left) and longitudinal (right) sections prepared from the middle segment of the seed. Bars = 1 mm for all images.

(B) Distribution of total TAG ions (sum of ions listed in Supplemental Table 1 online) normalized to the TIC on each pixel (max = 0.1 for both cross and longitudinal sections).

(C) Distribution of total PC ions (sum of ions listed in Supplemental Table 2 online) normalized to TIC on each pixel (max = 0.3).

(D) Distribution of total PA ions (sum of ions listed in Supplemental Table 4 online) normalized to TIC on each pixel (max = 0.03).

(E) Distribution of PE ions (sum of ions listed in Supplemental Table 3 online) normalized to TIC on each pixel (max = 0.01).

(F) Distribution of β -sitosterol ion (m/z 397.383) normalized to TIC on each pixel (max = 0.003).

(G) Distribution of gossypol (m/z 501.191) normalized to TIC on each pixel (max = 0.01).

differences, but it suggests a nonuniform distribution of TAG in cotton embryos as observed by MALDI-MSI.

Heterogeneous Distribution of Individual TAG Molecular Species

The most illuminating information obtained by MALDI-MSI of lipids came from examining the percentages of molecular species within classes. NMR-based imaging points to localized differences in seed lipid reserve accumulation within embryos, but it does not provide information about specific molecular composition. MALDI-MSI revealed the spatial organization of individual TAG molecular species (Figure 4) on the basis of mol % of total TAG. Individual TAG molecular species were identified as both Na^+ and K^+ adducts in MALDI-MSI full scans from a database of their theoretical monoisotopic masses established from literature sources (Yunusova et al., 1982; Líska and Holcapek, 2008; Horn et al., 2011a) and by comparison to ESI-MS data (see below).

Three distinct distribution patterns were identified within the TAG lipid class when comparing the molecular species distributions in cotton embryos. The two most abundant TAGs, PLL (m/z 877.726, Figure 4B) and LLL (m/z 901.726, Figure 4D), showed marked differences in location with less occurrence in the inner embryonic axis region relative to the outer cotyledon region. TAGs with two 16:0 acyl chains (e.g., PPL; m/z 853.725, Figure 4A) or one 16:0 and one 18:1 acyl chain (e.g., PLO; m/z 879.742, Figure 4C) were found to have a greater relative occurrence within the embryonic axis relative to cotyledonary tissues. A third distribution pattern that was relatively uniform throughout the entire embryo was evident for some TAGs, including LLO (m/z 903.742, Figure 4E). A more comprehensive list of TAGs identified is available in Supplemental Table 1 online.

Several cyclic FAs are found in cottonseeds in minor quantities, including sterculic, dihydrosterculic, and malvalic acids (Schmid and Patterson, 1988; Obert et al., 2007). Sterculic and dihydrosterculic acids are readily identifiable in odd chain TAGs. TAGs containing at least one 19C cyclic FA were exclusively localized in the embryonic axis of cotton embryos (Figure 5) and not detected in the outer cotyledonary regions representing a TAG distribution pattern distinctly different from TAGs without a cyclic FA. The minimum scale shown in Figure 4 is at least 20 times higher than the instrument detection limit, and if there is any TAG with a cyclic FA present in cotyledon, its abundance should be at least 20 times lower than that in embryonic axis. Gas

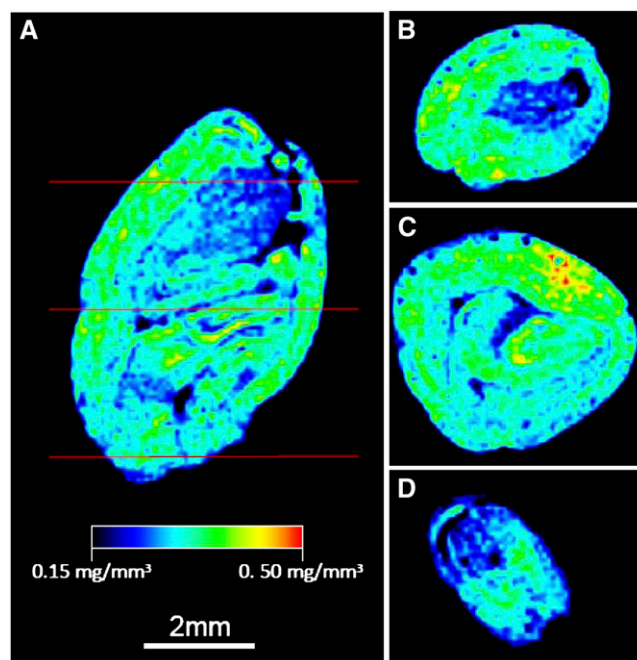


Figure 3. Distribution of Total Seed Lipid Content by NMR.

(A) Longitudinal representation of total seed lipids within an intact embryo. See Supplemental Movie 1 online for complete profiling of intact embryo.

(B) to (D) Representative cross-section profiles through the chalazal (B), middle (C), and micropylar (D) sections of the intact embryo.

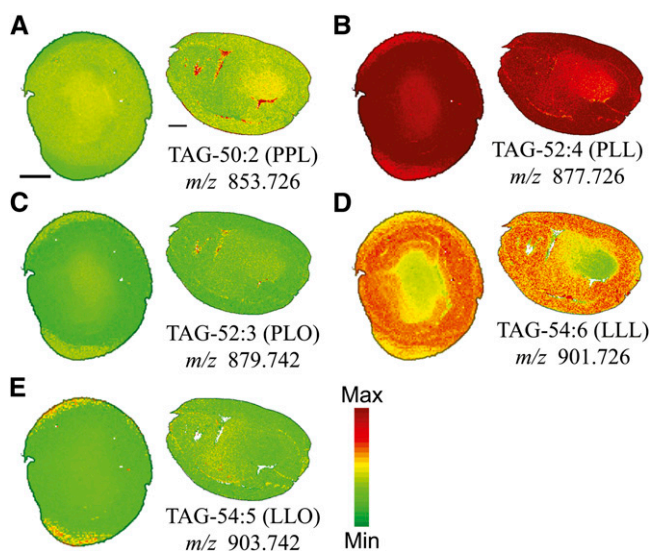


Figure 4. Distribution of Selected TAG Molecular Species.

Distribution of selected TAG molecular species in mol %. Ion counts within ± 0.02 m/z units of each sodiated $[M + Na]^+$ (labeled on figure) and potassiumated $[M + K]^+$ monoisotopic masses are normalized to the total TAG ion signals on each pixel. A red-green linear color scale is used with maximum mol % value corresponding to 35% of total TAG for all images. See Supplemental Table 1 online for all TAG species identified and m/z analysis for each species. Bar = 1 mm.

chromatography (GC)-MS analysis demonstrated the enrichment of cyclic FAs in the embryo axis and their near absence from the cotyledons (see Supplemental Figure 2 online). The most abundant species of these cyclic TAGs (LScP, LDscP/OScP, and ODscP) all contained one palmitic acid, one 18 carbon unsaturated FA (oleic or linoleic), and one sterculic or dihydrosterculic FA (Figures 5A to 5C). One of the less abundant cyclic TAGs contained two linoleic FAs and either sterculic or dihydrosterculic (Figure 5D). Malvalic acid is present in cottonseeds but has the same chemical formula and is not distinguishable from oleic acid by MS in full scan mode. Malvalic acid can be distinguished in derivatized FA profiles by GC-MS (Bao et al., 2002), but we were unable to obtain any information on TAGs with malvalic acid by MALDI-MSI here.

TAG molecular species were identified, and profiles were compared across analytical platforms at distinct tissue resolutions (Figures 6A and 6B): total lipid extracts (TLEs) from intact seeds, MALDI-MSI of seed sections, and direct organelle MS (DOMS) of purified cottonseed lipid droplets (Horn et al., 2011a). TLE and DOMS included quantitative standards and provided a reference basis for absolute quantification of TAG molecular species. TAG molecular species profiles were relatively similar across the different analytical platforms (Figures 6A and 6B), demonstrating the validity and utility of visualizing the lipid composition through MALDI-MSI. The cross and longitudinal sections revealed almost identical compositional profiles to each other, averaged from 20,000+ MS scans over entire embryo sections, and these were in good agreement with ESI-MS analyses.

The cyclic TAGs were more readily detectable in the longitudinal sections, but based on the optical images, it appears a slightly oblique cut was made that could lead to a larger portion of the embryonic axis being profiled. By comparison, cyclic TAGs appeared to be overestimated in direct-infusion ESI-MS of extracts. We suspect that this was due to the inability to resolve their m/z peaks with overlapping TAG species that appear as oxidized m/z artifacts. This overestimation of cyclic TAG in ESI-MS was evident following conventional total FA analysis of seed lipid extracts by GC-MS (Figure 6C; see Supplemental Figure 2 online), which were consistent with values from the literature (Schmid and Patterson, 1988; Obert et al., 2007). Hence, because of the high resolution of the Orbitrap-MS, analyses by MALDI-MSI were able to resolve these oxidized species and exclude them from relative quantification calculations, making MALDI-MSI a better representation of cyclic TAG content in embryos than ESI-MS approaches in this case and emphasizing the importance of comparing multiple methods to verify lipidomics results.

Stereospecific designations (i.e., *sn*-position of each FA) were not determined in our analyses but have been shown to be possible in ESI-MS/MS of TLEs (Han and Gross, 2001). The MALDI-MSI instrument used in this study has MS/MS capability, and we have previously shown structural isomers can be distinguished in MALDI-MS/MS imaging (Perdian and Lee, 2010). Here, however, molecular species were distinguished only by overall acyl composition (numbers of acyl carbons and numbers of double bonds).

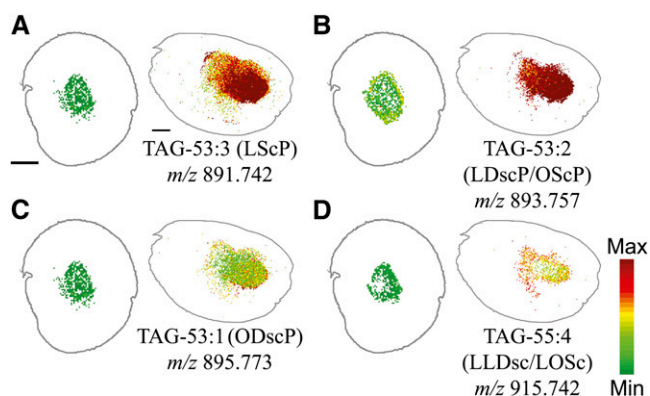


Figure 5. Distribution of TAG Molecular Species Containing Sterculic and/or Dihydrosterculic (Cyclic) Fatty Acids.

Distribution of selected cyclic TAG molecular species in mol %. Ion counts within ± 0.02 m/z units of each sodiated $[M + Na]^+$ (labeled on figure) and potassiumated $[M + K]^+$ monoisotopic masses are normalized to the total TAG ion signals on each pixel. A red-green linear color scale is used with maximum mol % value corresponding to 3% of total TAG for all images. See Supplemental Table 1 online for all cyclic TAG species identified and m/z analysis for each species. Bar = 1 mm.

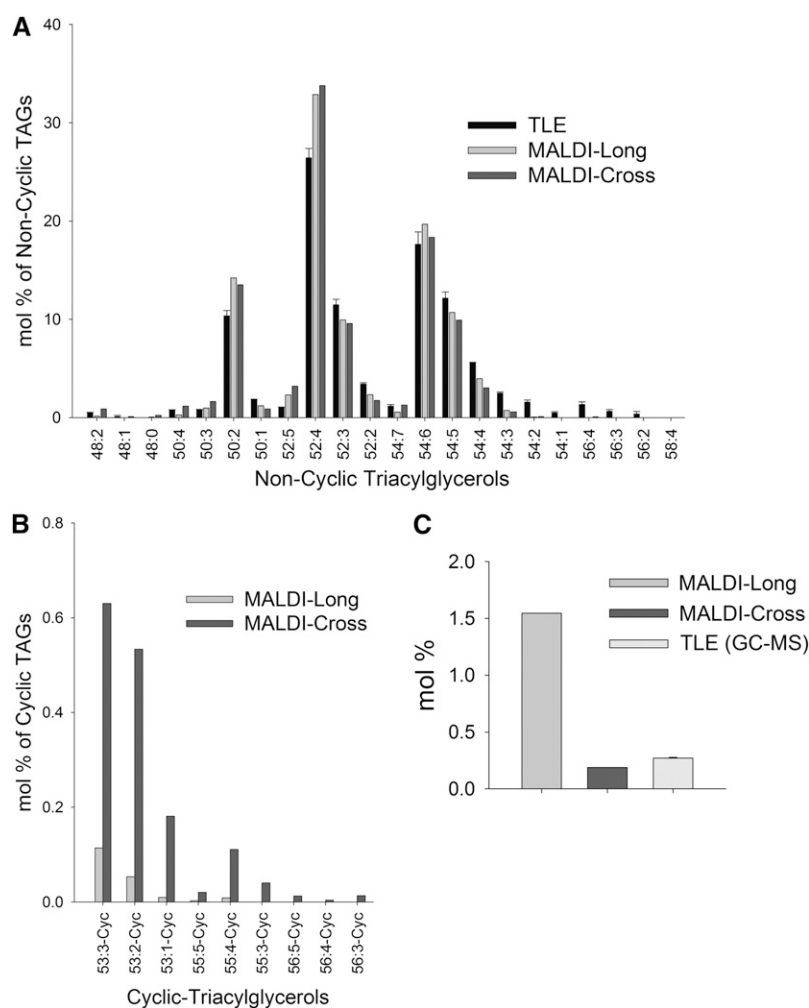


Figure 6. Comparison of TAG Molecular Species Profiles at Different Spatial Resolutions.

(A) Individual noncyclic TAG species were quantified as mol % of total TAG content: (1) at tissue resolution – TLE of mature embryos sampled through direct-infusion ESI-MS ($n = 3$); or (2) at cellular resolution – MALDI-MSI longitudinal and cross sections. These data are in agreement with results from DOMS of small lipid droplet populations ($n = 3$ sets of 10 to 25 lipid droplets) (Horn et al., 2011a). See Supplemental Table 1 online for all noncyclic TAG species identified and m/z analysis for each species.

(B) Mol % distribution of TAGs with one or more acyl cyclic FAs (sterculic and/or dihydrosterculic) normalized to total TAG content in MALDI-MSI sections. See Supplemental Table 1 online for all cyclic TAG species identified and m/z analysis for each species.

(C) Comparison of total 19C cyclics quantified by MALDI-MSI and GC-MS. For MALDI sections, 19C cyclic TAGs (sterculic + dihydrosterculic) were normalized to total TAG content. For GC-MS analysis, TLEs were converted to FAMES with total 19C cyclic FAs (sterculic + dihydrosterculic) normalized to total FA content ($n = 3$). See Supplemental Figure 2 online for total FA composition quantified by GC-MS.

Heterogeneous Distribution of Individual PC Molecular Species

PC is one of the most frequently analyzed lipid classes in MALDI-MSI due to its abundance, matrix compatibility, and ease of ionization (Zabrouskov et al., 2001). Total PC distribution (Figure 2C) in the cross and longitudinal sections of cotton embryos was relatively homogenous with a slight reduction in PC within the embryonic axis. However, individual PC molecular species showed some substantial differences in tissue distribution when calculated as a mol % of the total PC (Figure 7). The two most abundant PC molecular species, PC-36:4 (m/z 782.571,

Figure 7C) and PC-34:2 (m/z 758.571, Figure 7A), were enriched within the cotyledons compared with the embryonic axis. The difference in PC-36:4 (LL) distribution was more pronounced than PC-34:2 (PL), reminiscent of the patterns found in the major TAG molecular species, TAG-54:6 (LLL, Figure 4D) and TAG-52:4 (PLL, Figure 4B). The presence of 18:1 within a PC molecular species reversed the relative distribution patterns to where the embryonic axis was more enriched: for example, PC-36:3 (LO, m/z 784.586, Figure 7D versus 7C) and to a lesser degree PC-34:1 (PO, m/z 760.585, Figure 7B versus 7A). The same trend was also found in TAG; the replacement of L with O resulted in

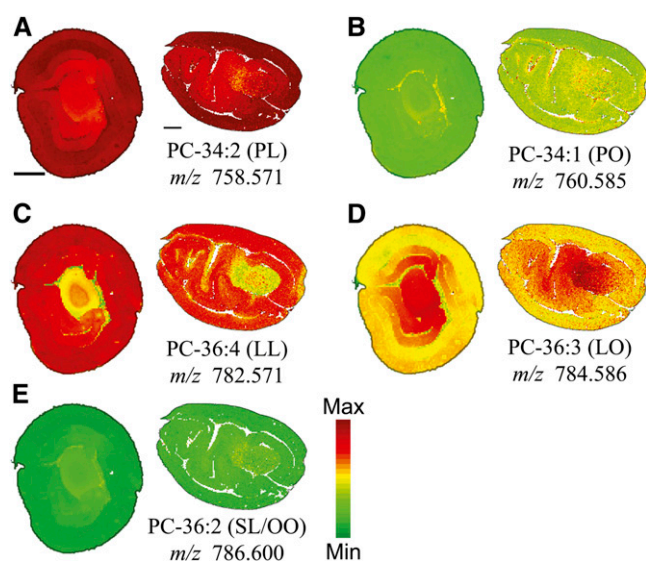


Figure 7. Distribution of Selected PC Molecular Species.

Distribution of selected PC molecular species in mol %. Ion counts within ± 0.02 m/z units of each protonated $[M + H]^+$ (labeled on figure), sodiated $[M + Na]^+$, and potassiumated $[M + K]^+$ monoisotopic masses are normalized to the total PC ion signals on each pixel. A red-green linear color scale is used with a maximum mol % value corresponding to 35% of total PC for all images. See Supplemental Table 2 online for all PC species identified and m/z analysis for each species. Bar = 1 mm.

reversed or even distribution patterns between the cotyledons and axis (PLL versus PLO and LLL versus LLO). The relative average quantities determined by MALDI-MSI of each molecular species of PC in both cross and longitudinal sections were similar to distributions quantified in TLEs by ESI-MS (Figure 8). Unlike cyclic TAGs, cyclic PCs were slightly more abundant in the cross sections compared with longitudinal sections relatively speaking, but in both cases, cyclic PCs were localized almost exclusively within the embryonic axis (Figure 9). A comprehensive list of PCs identified by MALDI-MSI is available in Supplemental Table 2 online.

In *Sterculia foetida*, where cyclopropenoic FAs are found up to 65 to 78% in seeds, there is evidence that the cyclopropane FA synthase enzyme synthesizes dihydrosterculate by an addition of a methyl group (from *S*-adenosyl-L-Met) at the delta-9, 10 position of oleate esterified at the *sn*-1 position of a PC molecule (Bao et al., 2002). Desaturation of dihydrosterculate to produce sterculate then occurs by a cyclopropane FA desaturase that is less characterized (Bao et al., 2002). Therefore, 19C cyclic FA on PC serves as the precursor source for cyclic FA transferred to TAG molecules as for other acyl moieties. Similar to the cyclic-TAG molecular species imaged in cottonseeds, the PC molecular species with a sterculic or dihydrosterculic FA were almost exclusively found in the embryonic axis of embryos (Figure 9) consistent with previous reports that radicle tips were enriched in cyclic FAs (Schmid and Patterson, 1988). Several cyclic PC molecular species were identified that contain one linoleic acid or palmitic acid and either a sterculic or dihydrosterculic acid (Figures 9A to 9E). The colocalization in the embryonic axis of cyclic

PC and cyclic TAG molecular species reinforces the important ability with imaging MS to visualize the spatial relationships of metabolites, especially where engineering elevated levels of industrial lipids (like cyclic FAs) might be desirable (Liu et al., 2009).

Graphical Representation of Lipid Distributions

An alternative approach to visualizing the distribution of molecular species within a lipid class by MALDI-MSI was to plot the mol % values relative to their x and y position (i.e., Figures 4, 5, 7, and 9). Traversing across the tissue sections (Figure 10A) represented two distinct tracks through developmentally and functionally different tissues. TAG and PC molecular species showed remarkably variable distribution patterns across the x axis (Figures 10B and 10C), especially between cotyledons and the embryonic axis. Despite being sectioned in different orientations, cross and longitudinal sections showed similar distribution patterns of TAG and PC relative to one another. These graphical distribution-type profiles, obtained from individual scans averaged at each location, can be adapted to the analysis of other metabolites and will be valuable in other studies for showing metabolite changes as a result of developmental maturity, cell type differences, or responses to environmental stresses.

Imaging Other Membrane and Signaling Lipids

PE is a common membrane phospholipid that contains a free amino group at the polar end of the molecule, unlike PC. Acyl groups on PE molecular species are not direct substrates for TAGs, but PE and PC share a biosynthetic route and potential diacylglycerol precursors in the ER. We were curious if this lipid class could be ionized and imaged in MALDI-MSI, given that embryos had been lightly fixed prior to sectioning. Indeed, PE molecular species distributions in embryos were profiled readily

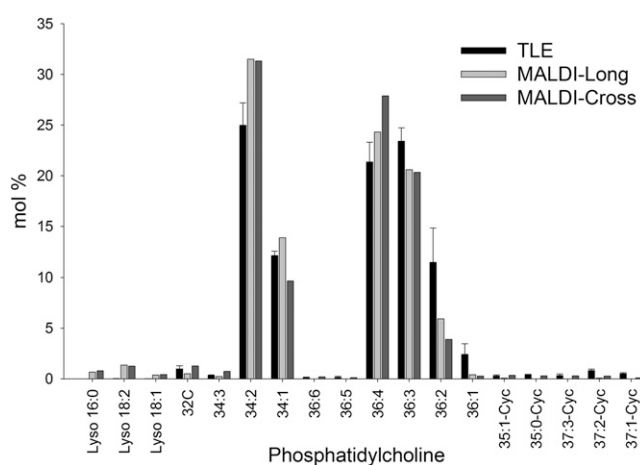


Figure 8. Comparison of PC Molecular Species from MALDI-MSI Sections and TLEs.

Individual PC species were quantified as mol % of total PC content for MALDI-MSI sections and by direct-infusion ESI-MS of the polar lipid fraction (purified through solid-phase extraction) of total embryo lipid extracts ($n = 3$).

by MALDI-MSI (Figure 11), and profiles were in reasonably good agreement with those obtained by quantitative, shotgun ESI-MS (Figure 11C). Although fewer major molecular species of PE were identified than for PC (cf. Supplemental Tables 2 and 3 online), some of the major species corresponding to the dominant PE species could be identified. Molecular species profiles of PE displayed a heterogeneous distribution (Figure 11) but different than might be predicted if PC and PE biosynthesis were coincident. PE-34:2 and PE-36:4 were distributed different from one another (Figure 11), demonstrating heterogeneity within the PE lipid class like that for other glycerolipids. Interestingly, PE-34:2 was distributed coincident with PC-34:2, more enriched in cotyledons than the axis. On the other hand, PE 36:4 was enriched in interior tissues of embryos, opposite the distribution of PC-36:4 (cf. Figures 7C and 11C), suggesting that there is an unequal utilization of DAG-36:4 precursors for these two membrane lipids in these two different tissues of the embryo, a concept that might have gone unrecognized without the ability to localize specific membrane lipid species together in situ.

PC and PE are abundant membrane lipids, but some membrane lipids occur in much lower concentrations like PA, which functions as both an intermediate in TAG biosynthesis and an important signaling molecule in various stress responses (Testerink and Munnik, 2005; Wang et al., 2006). Here, we imaged the prevalent PA molecular species in cottonseeds (Figure 12). The major molecular species of PA was PA-36:3 (see Supplemental

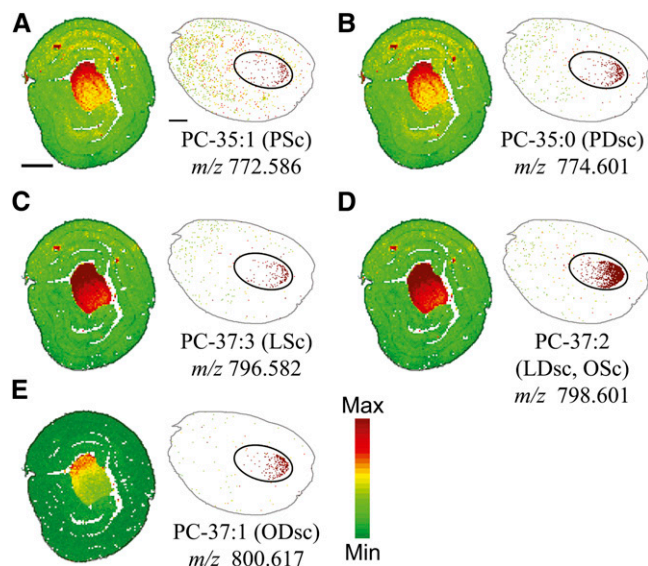


Figure 9. Distribution of PCs Containing Steric and/or Dihydrosteric FAs.

Distribution of selected cyclic PC molecular species in mol %. The embryonic axis is outlined in the longitudinal sections to emphasize the localization of cyclic PCs. Ion counts within ± 0.02 m/z units of each sodiated $[M + Na]^+$ (labeled on figure) and potassium $[M + K]^+$ monoisotopic masses are normalized to the total PC ion signals on each pixel. A red-green linear color scale is used with a maximum mol % value corresponding to 1% of total PC for all images. See Supplemental Table 2 online for all cyclic PC species identified and m/z analysis for each species. Bar = 1 mm.

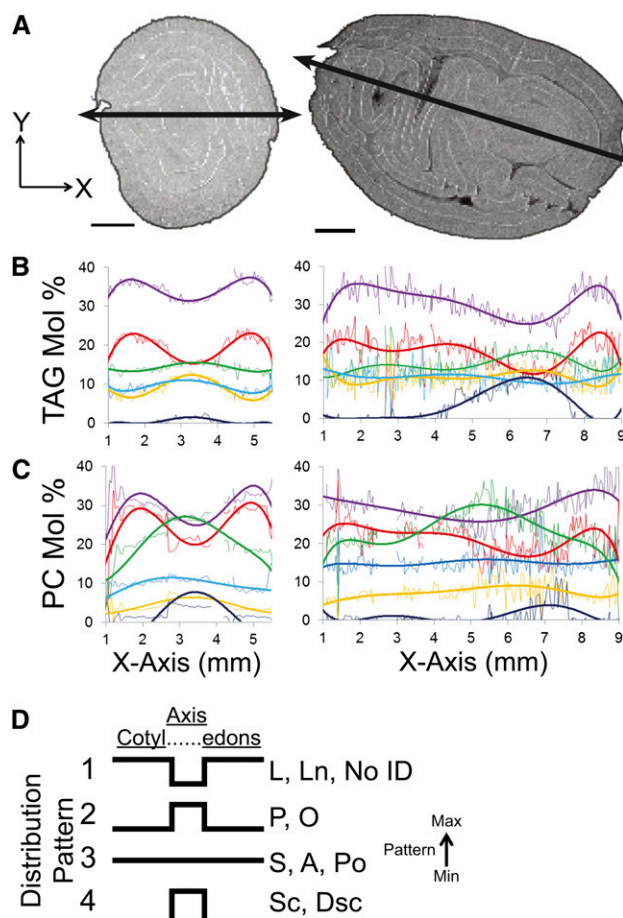


Figure 10. Distribution of TAG, PC, and Corresponding FA Species across MALDI-MSI Sections.

(A) TIC distribution of cross and longitudinal sections. The line drawn through the sections represents the set of x, y coordinates analyzed for their TAG and PC relative molecular distributions (i.e., each pixel traversed across will have a MALDI-MSI spectrum associated with it). Bars = 1 mm. **(B)** Distribution of selected TAG species across the center of the cross-section plotted relative to their x axis location. Thin lines represent the individual mol % values at that x, y position for a particular species (purple, TAG-52:4 PLL; red, TAG-54:6 LLL; green, TAG-50:2 PPL; yellow, TAG-52:3 PLO; light blue, TAG-54:5 LLO; dark blue, combined steric/dihydrosteric cyclic TAGs). Thick lines represent a polynomial fit using Microsoft Excel to aid visualization of changes across the section.

(C) Distribution of selected PC species across the center of the cross section plotted relative to their x axis location. Thin lines represent the individual mol % values at that x, y position for a particular species (purple, PC-34:2 PL; red, PC-36:4 LL; green, PC-36:3 LO; yellow, PC-36:2 LS/OO; light blue, PC-34:1 PO; dark blue, combined steric/dihydrosteric cyclic PCs). Thick lines represent a polynomial fit using Microsoft Excel to aid visualization of changes across the section.

(D) Summary of FA distribution patterns relative to their mol % contribution of the cross and longitudinal sections. Four distinct distributions patterns were present throughout the seed sections. Pattern strokes represent relative abundances for identified FAs: P-16:0, palmitic; Po-16:1, palmitoleic; Ln-18:3, linolenic; L-18:2, linoleic; O-18:1, oleic acid; S-18:0, stearic; A-20:0: arachidic; Sc-19:1 steric acid; Dsc-19:0-dihydrosteric acid; as well as those without identification (No ID).

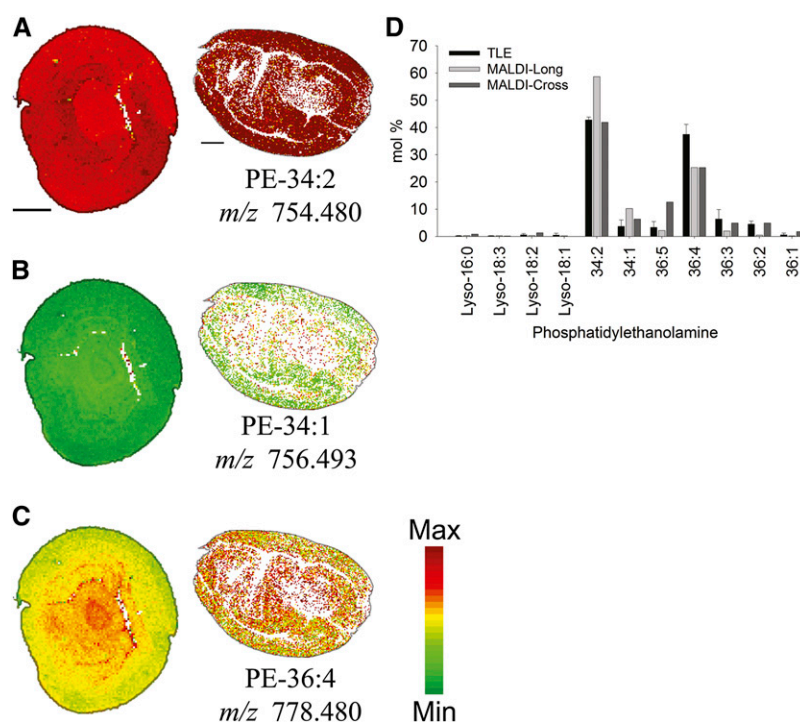


Figure 11. Distribution of Selected PE Molecular Species.

(A) to (C) Distribution of selected PE molecular species in mol %. Ion counts within ± 0.02 m/z units of each potassiumated $[M + K]^+$ (labeled on figure), protonated $[M + H]^+$, and sodiated $[M + Na]^+$ monoisotopic masses are normalized to the total PE ion signals on each pixel. A red-green linear color scale is used with a maximum mol % value corresponding to 50% of total PE for all images. See Supplemental Table 3 online for all PE species identified and m/z analysis for each species. Bar = 1 mm.

(D) Comparison of PE molecular species from MALDI-MSI sections and polar lipid fractions (purified through solid-phase extraction) of TLEs analyzed by direct infusion ($n = 3$).

Table 4 online for all PA species identified), and it was distributed throughout the embryo with a greater relative percentage in the cotyledons. This acyl composition of the major PA species in embryos was not a reflection of the major TAG species in the cotyledon regions (LLL and PLL; Figure 4) and was opposite the distribution of PC-36:3 (potential precursor; Figure 7), which was more concentrated in the axis of the embryo. Several of the minor PA species showed some interesting apical/basal polarity in distribution within the embryo (Figure 12). For example, the PA 34:2 in longitudinal sections appeared to be enriched in micro-pylar regions of the embryo (Figure 12A, bottom right). While the functional significance of differences in PA species distributions remains to be elucidated, it appears from the species imaged here that the PA connection in these desiccated seeds is not one to TAG metabolism (which is most active during the embryo maturation stage) but rather may be linked to signaling functions of PA related to seed germination. These results indicate that lipids with known signaling functions can be imaged by MALDI-MSI and open the possibility of studying lipid signaling within a cellular context.

DISCUSSION

Visualizing the dynamic complexity of lipid metabolism at cellular resolution is not currently achievable with conventional, extraction-

based lipidomics. In this study, we adapted MALDI-MSI to uncover the detailed molecular distribution of major storage and membrane lipid classes in tissues of mature cotton embryos. Even minor membrane lipids and other types of lipid-soluble metabolites were able to be imaged by MALDI-MSI. Remarkable cell-type/tissue-specific variation was observed throughout the embryo in the composition of TAG, PC, PE, and PA molecular species, but there were discernible, apparently related, patterns based on acyl moieties in PC and TAG (Figures 4, 5, 7, 9, and 10). Individual TAG and PC molecular species with similar FA compositions had similar MALDI-MSI distribution profiles (Figure 10), which is not surprising given the metabolic relationship between PC and TAG (Chapman and Ohlogge, 2012). More unexpectedly, we found that species with polyunsaturated FAs (almost all linoleic in cottonseed) were found at higher relative abundances in the cotyledon regions of the embryo relative to the embryonic axis (see Supplemental Figure 2 online). This was opposite for palmitic and oleic acids, which contributed proportionally more to glycerolipid species found within the embryonic axis. Lipids containing the less abundant stearic, arachidic (20:0), and palmitoleic (16:1) FAs were found uniformly distributed throughout the embryo (Figure 10D). Finally, sterculic and dihydrosterulic acids (cyclic FAs) were localized almost exclusively in the embryonic axis (see Supplemental Figure 2 online). The differences

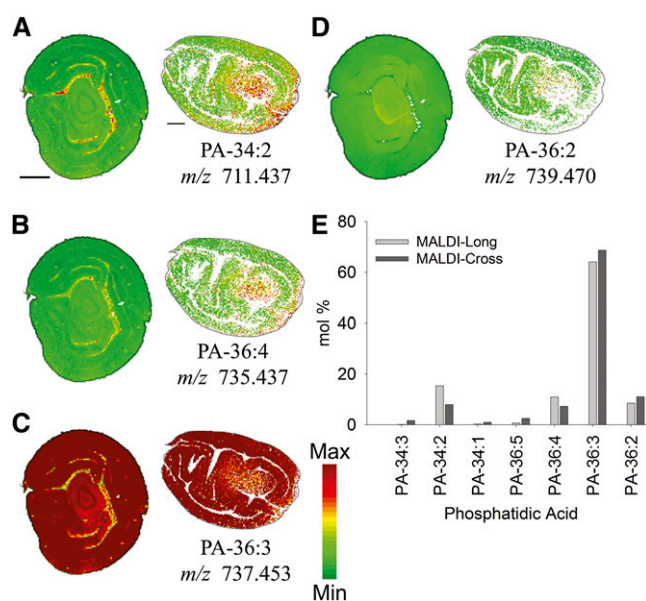


Figure 12. Distribution of Selected PA Molecular Species.

(A) to (D) Distribution of selected PA molecular species in mol %. Ion counts within ± 0.02 m/z units of each potassiumated $[M + K]^+$ (labeled on figure) and sodiated $[M + Na]^+$ monoisotopic masses are normalized to the total PA ion signals on each pixel. A red-green linear color scale is used with a maximum mol % value corresponding to 60% of total PA for all images. See Supplemental Table 4 online for all PA species identified and m/z analysis for each species. Bar = 1 mm.

(E) Comparison of PA molecular species from MALDI-MSI sections.

in molecular distribution of lipids are most certainly a consequence of differential gene expression and enzyme localization but also may imply differences in localized function beyond metabolic precursor/product relationships (i.e., PC-36:3 versus PC-36:4 or PA-36:3 versus PA-34:2).

The information here about the heterogeneous distribution of lipids in cotton embryos is surprising but is consistent with the results from recent work with organellar lipidomics from cotton embryos (DOMS). DOMS of individual lipid droplets revealed that lipid droplets in cottonseed embryos displayed a remarkable organelle-to-organelle difference in TAG composition, yet when these different compositions were averaged together, they resembled the overall composition of cottonseed oil (Horn and Chapman, 2011; Horn et al., 2011a). Individual lipid droplets showed distinctly different compositions of TAG molecular species. Now these compositions of individual droplets can be explained at the level of regional heterogeneity within the embryos. For example, one droplet contained 17% PPL, 26% PLL, 14% PLO, 12% LLL, and 10% LLO. This composition is consistent with the TAG molecular species composition range imaged by MALDI-MSI in the embryonic axis region (Figure 10). Hence, heterogeneity at the subcellular organelle level in lipid droplets from cottonseeds likely is contributed to by the regional differences in TAG synthesis and packaging in cottonseed embryos. The overall concept of cellular heterogeneity presents new challenges when considering cellular biochemistry in multicellu-

lar organisms. Further work will be needed to understand the precise mechanisms regulating these compositional differences at the cellular level, but this type of information may be important to predicting and defining limitations in metabolic engineering strategies.

The assembly of TAGs in oilseeds involves multiple pathways and subcellular compartments (Bates et al., 2009; Chapman and Ohlrogge, 2012). FAs destined for incorporation into TAGs are synthesized in the plastid and exported (mostly as 16:0 and 18:1 FA) to the ER as part of an acyl-CoA pool. Acyl groups are used for glycerolipid synthesis in the ER by enzymes of the Kennedy pathway that provide DAG backbones for PC synthesis or for TAG synthesis. Alternatively, acyl-CoAs can be incorporated rapidly into PC independent of the Kennedy pathway (Bates et al., 2009). Acyl modification, including desaturation and cyclopropane addition, occurs in FAs esterified to PC (Sperling et al., 1993; Bao et al., 2002), so there is a dynamic and close relationship between acyl groups on PC and acyl groups in TAG. FA can be shuttled to TAGs through a number of different pathways: (1) acyl-CoA-dependent acyltransferases that assemble TAG on the glycerol backbone (Stymne and Stobart, 1987); (2) an acyl-CoA-independent mechanism for synthesizing TAGs (especially with usually FAs) through phospholipid:DAG acyltransferase (Dahlqvist et al., 2000); (3) an acyl editing mechanism between the acyl-CoA pool and PC via lysoPC acyltransferase or phospholipase A (Stymne and Stobart, 1984); and/or (4) the transfer of the phosphocholine head group between PC and DAG by PC:DAG cholinephosphotransferase to supply unsaturated DAG for TAG synthesis (Lu et al., 2009).

Consequently, molecular species information for PC and TAG in cotton embryo tissues may help to predict unforeseen spatial differences in the pathways, genes, and enzymes responsible for the assembly of cottonseed TAG. For example, the identification of PC-36:3 with one 18:1 acyl chain in the embryonic axis suggests that this species is the source of 18:1 for the cyclopropane FA synthase and desaturase that is then transferred as cyclic FA to TAG. Also, the higher levels of linoleic acid in PC and TAG in the cotyledon tissues suggests there is a difference in delta-12 desaturase (FAD2) enzyme distribution with cottonseeds, and it is likely that a PC:DAG cholinephosphotransferase activity also functions in these tissues to enrich polyunsaturated FA in TAG (e.g., LLL and PLL). Addressing these types of questions at different stages of development or in combination with transgenic experiments and expression studies will lead to new insights into the cellular regulation of lipid synthesis in oilseeds. By extrapolation, studies of lipid metabolism by MALDI-MSI in other plant tissues or in different environmental conditions will extend a new perspective to the importance of lipid localization and function.

The major molecular species of PE and PC are not exactly similar in cottonseeds (Figures 8 and 10). However, curiously, even the mol % distributions were differentially localized between the two major molecular species of PE and PC that had the same diacylglycerol moiety. For PC-36:4 and PE-36:4 (both di-18:2), the distributions were opposite; PC-36:4 made up a larger mol fraction of total PC in the cotyledons than in the axis, whereas PE-36:4, although distributed throughout the embryo, appeared to make up a larger proportion of the total PE class

within regions of the embryonic axis. By contrast, PC-34:2 and PE-34:2 (both 16:0/18:2) appeared to have a similar, somewhat uniform, distribution to one another, although PC-34:2 was slightly more concentrated in cotyledonary tissues than in the axis tissues, relatively speaking. These differences in location may imply differences in function, but they are perplexing in terms of our views of PC/PE biosynthesis, since the diacylglycerol moieties for both of these phospholipid classes are believed to be assembled in the same subcellular compartment. Does this reflect differences in substrate preferences between choline- and ethanolamine-phosphotransferases? Why is so little PE-36:3 made at all when PC-36:3 is a major PC molecular species concentrated within the embryonic axis? These results seem to point to an unknown level of compartmentation (and perhaps enzyme distribution/specificity) for membrane lipid biosynthesis that only now can be appreciated.

The mass accuracy and dynamic range of the LTQ-Orbitrap mass spectrometer interfaced with MALDI ionization supported the identification and characterization of a large number of lipid compounds in cotton embryos. There remains a wealth of chemical information to be mined from MS imaging data. In typical MALDI-MSI spectra, there were multiple adducts (i.e., H^+ , K^+ , and Na^+) for each lipid molecular species that substantially increased the number of detectable compounds 2 to 3 times that of direct-infusion ESI-MS with a single adduct. For PC and TAG species, most of these peaks could be separated from the surrounding other peaks by accurate mass measurements. The comparisons of spectra from MALDI-MSI with those from traditional chemical-based extracts analyzed by ESI-MS/MS were extremely valuable for compound identifications and should be employed in the analysis of other plant tissues by MALDI-MSI. MALDI-MSI yielded spectra with many peaks that have yet to be identified, indicating the need for algorithms to identify novel compound candidates that, because of their stability, localization, or concentration, are not otherwise possible to identify by ESI-MS/MS. The wide dynamic range of the instruments used permitted the detection of low-abundance cyclic FAs esterified to PC (e.g., most abundant cyclic PC is 1% of total PC, which itself is only $\sim 2\%$ of total lipid, which itself is $\sim 20\%$ oil of total seed weight or $\sim 0.0004\%$ of the total seed weight). Detection of minor lipid species makes it likely that lipids functioning as signaling molecules may be able to be localized by MALDI-MSI in the future.

By way of example, the profiles of PA were determined in cottonseed sections. Amounts of PA are normally low in plant tissues, and this lipid can serve as an intermediate in TAG biosynthesis or as a central lipid mediator in signal transduction pathways (Testerink and Munnik, 2005; Wang et al., 2006). The distribution of PA species in embryos was intriguing, and based on comparisons of acyl composition of PA, PC, and TAG, the PA in desiccated seeds did not appear to be a reflection of metabolic flux to TAG. PA molecular species composition was dominated by PA 36:3, and this was distributed throughout the cotyledonary and embryonic axis tissues, with perhaps less relative representation in the axis region (based on mol % of total PA). This is in sharp contrast with the distribution of TAG and PC species that contain the combinations of 18:1 and 18:2 FA (Figures 4, 7, and 10). It is likely that direct-infusion lipidomics analysis of total seed

extracts would have revealed this same information, but what would be entirely obscured in tissue extractions is the apparent polar distributions of certain PA molecular species. The PA composition within the hypocotyl-root axis and the micropylar regions of the cotyledonary tissues of the embryo were very different from the rest of the embryo. Several relatively minor species were much more concentrated in these regions. PA has been shown to interact with the abscisic acid regulation of seed germination and postgerminative growth (Katagiri et al., 2005), and these PA species and their distribution in the radicle near the location of radicle protrusion may indicate a role in seed biology more related to signaling than TAG metabolism. Of course this speculation remains to be tested experimentally, but questions would not have been considered without knowing the heterogeneous localization of PA molecular species. Furthermore, these results point to the realistic possibility of imaging other signaling lipids and molecules for localized effects in plant tissues, opening up a new approach to visualizing signal transduction directly at the chemical and cellular levels.

Several considerations were addressed when evaluating the veracity of the MALDI-MSI approach in seed sections. Analysis of PC and TAG (and other lipid classes) together by MS is known to be difficult due to ion suppression phenomena (Emerson et al., 2010). Ion suppression makes quantitative conclusions tenable without the addition of internal standards, as is routine in direct-infusion lipidomic analyses. Here, we observed clear evidence of ion suppression in MALDI-MSI where ion intensities for TAG species were much less overall than for PC species despite the fact that there is ~ 50 times more TAG than PC in cottonseeds. Therefore, it is not prudent to interpret quantities of lipid classes directly from ion intensities in these MALDI-MSI spectra. This caution is reinforced when comparing the images from total ion distribution (Figure 2) to images of total lipid distribution by 1H -NMR (Figure 3). NMR-derived images of cottonseed lipids, like those for soybean (Neuberger et al., 2008), showed most of the seed oil in cotyledon tissues relative to the embryonic axis (Figure 3). This appeared to be the reverse in ion intensity profiles by MALDI-MSI (Figure 2B). However, PC was relatively more abundant in cotyledon tissues of cotton embryos (Figure 2C), and we presume that signals from TAG were relatively more suppressed by PC in these regions. The future development of methods to include internal standards within the sample matrix may help to improve the quantitative nature of imaging *in situ*. Nonetheless, it was still possible to obtain relative composition information within lipid classes by MALDI-MSI. This was confirmed by comparing MS scans averaged across sections where mol percentages of TAG molecular species (Figure 7) were in excellent agreement with those obtained by quantitative, direct-infusion ESI-MS/MS of lipid extracts, or by DOMS of isolated cottonseed lipid droplets (Horn et al., 2011a). Similar results were observed for PC species profiles (Figure 10). There may be an overrepresentation of cyclic FA species in ESI-MS, but, in general, the TAG and PC lipid compositions by MALDI-MSI were similar to those obtained by conventional quantitative techniques, and these were all in good agreement with values reported in the literature for cottonseed lipid species quantified by other methods (e.g., high performance liquid chromatography/thin layer chromatography/GC; Lisa and Holcapek, 2008;

Dowd et al., 2010; Dowd, 2011). It should be noted that the same approach has been taken by Murphy and coworkers in comparison of each PC molecular species of rat brain cross sections between MALDI-MSI and liquid chromatography–MS/MS analysis, and quantitative agreement was found regardless of the tissue type (Hankin and Murphy, 2010). We conclude that by examining the mol fraction of individual species within lipid classes, MALDI-MSI is an accurate representation of lipid distribution within sections of plant tissues.

In expanding applications of MALDI-MSI to other types of plant tissues, attention will need to be placed on sample preparation and the balance between structural and chemical integrity. First of all, according to our and others' experiences, polymer embedding materials cannot be used for soft plant tissues in cryosectioning because they penetrate into the tissues and produce significant polymer contaminations in MS measurements. Other materials, such as ice and gelatins, are suggested in those cases (Chughtai and Heeren, 2010). We could still use optimal cutting temperature polymers in hard tissues like cottonseeds, but we had another issue of surface smearing during the cryosectioning. Hence, we fixed the embryos with paraformaldehyde before cryosectioning to preserve the tissue integrity. It should be emphasized here that chemical profiles for lipids were not different between unfixed and lightly fixed seed tissues. Also, lipid molecular species profiles by MALDI-MSI were in good agreement with those obtained from TLEs by ESI-MS. This was even the case for PE, which has a free amino group and might be expected to be susceptible to fixation by formaldehyde. So while fixation might present a problem in the profiling of proteins, we do not consider this to be a major issue for lipid imaging by MALDI-MSI. However, it is possible that other targeted lipid classes or species may be impacted adversely by chemical fixation or embedding procedures, and suitable methods may need to be developed to broaden the range of compounds that can be imaged by MALDI-MSI. In any case, the major value of knowing the spatial distribution of chemical compositions in plants will likely drive development of new approaches that combine MS-based analysis with cellular and even subcellular imaging, and these efforts will form the basis for improved understanding of plant biochemistry at higher resolution.

METHODS

Cottonseed Material

Cotton (*Gossypium hirsutum* cv Coker 312) plants grown in soil were maintained at 30°C in an air-conditioned greenhouse supplemented with Na-vapor lamps for an extended daylength of 16 h. Seeds were harvested from mature bolls and delinted in a tabletop, 10-saw laboratory gin. Intact mature embryos were excised from the seed coat with a standard razor blade in preparation for sectioning or chemical extraction.

Sample Preparation for MALDI-MS Imaging

Mature cotton embryos were either unfixed or lightly fixed with 4% paraformaldehyde for 30 min to preserve structural characteristics during sectioning. Excess fixative was washed off the seeds with three successive 5-min washes in 50 mM PIPES-NaOH, pH 7.2. Seeds were mounted

on a minimal amount of optimal cutting temperature polymer (Sakura Finetek) and then covered with the optimal cutting temperature polymer completely. The samples were flash frozen with powdered dry ice on a cryostat holder, covered with an aluminum foil, and maintained at –80°C for 10 to 15 min. Seeds were sectioned in a cryostat (Leica 1800 cryocut) at –20°C, and 30- μ m sections in cross-orientation or longitudinal orientation relative to the embryonic axis were collected on glass slides and placed in evacuated desiccators at room temperature until ready for shipment to Iowa State University for analysis. Samples were stored in desiccators at Iowa State University until ready for MSI analysis.

MSI

The 2,5-Dihydroxybenzoic acid (Sigma-Aldrich) was applied by sublimation, using a procedure adapted from Hankin et al. (2007). MS imaging was conducted using a MALDI linear ion trap-Orbitrap hybrid mass spectrometer (MALDI LTQ Orbitrap-Discovery; Thermo Fisher Scientific). Spectra were collected using the Orbitrap analyzer with Xcalibur (v.2.0.7) data acquisition software. The instrument was equipped with an intermediate pressure (75 mTorr) MALDI source using a nitrogen laser (MNL 100; Lasertechnik Berlin), providing an output at 337 nm with a maximum energy of 80 μ J per pulse and a repetition rate of 60 Hz (Strupat et al., 2009). A 3-mm aperture was placed in the beam path to reduce the spot size at the sample surface to 35 to 40 μ m, as measured by inspection of burn marks on a thin film of α -cyano-hydroxycinnamic acid (Qiao et al., 2008). MS images were collected for the selected area in the positive ion mode with a 50- μ m raster step size. The Orbitrap analyzer was used for MS data acquisition at the nominal resolution of 30,000. Automatic gain control was turned off, and other data acquisition conditions were optimized each time. Typical experimental conditions were as follows: laser power per pulse of 5 to 10 μ J, the number of laser pulse per spectra of one to five, and the number of scans averaged per pixel of 3 to 10. To avoid damage to tissue sections used for imaging, sections prepared in parallel to those imaged were used for this optimization.

Processing for MSI

Raw spectra files acquired from the Orbitrap analyzer were converted to .txt files using the Xcalibur 2.0.7 conversion feature for further processing with a custom, in-house Java MALDI-imaging analysis application, LipidImager. The text version retains all spectral information in a format suitable for further analysis with LipidImager. Each MALDI mass scan (or set of scans) represents an absolute position (i.e., with x , y coordinates) analyzed within the seed section. Individual scans, or an averaged set of scans, at a particular x , y position were processed to search for compounds of a desired m/z within tolerance limits of 0.02 D. This tolerance was selected based on the high resolving power of the Orbitrap analyzer and refined through rounds of m/z analysis of peaks identified (see Supplemental Tables 1 to 4 online).

Several adducts were found for each lipid class analyzed (see Supplemental Tables 1 to 4 online). TAGs were detected as both sodium and potassium adducts with both being used to generate chemical images of TAGs. Mol percentages within a particular lipid class at an x , y position were calculated based on absolute intensities of identified compounds relative to the total ion intensity summed for the lipid class (see example calculation in Supplemental Figure 1 online). Since no internal standards were able to be added, absolute quantities (e.g., μ g) were not calculated. MALDI-MS images were generated in Java by converting the x , y coordinates associated with each scan and the corresponding mol % of a particular compound at that location into a colored-square pixel according to a gray or green-to-red color scale (see example in Supplemental Figure 1 online). Distribution profiles of sections were generated from a known absolute x , y position of a scan (or set of scans) and the pixels representing the mol % (or TIC) at that point. Scale bars were

automatically generated by converting the absolute size of the pixel representation used for each image. Using an optical image from each type of section, an outlined template was overlaid onto each MALDI image in Adobe Photoshop CS4.

Total Lipid Determination by Magnetic Resonance Imaging

The NMR imaging experiments were performed using a Bruker 750 WB Micro Imaging System (Bruker) equipped with a 20-mm birdcage coil. To visualize the lipids within the seed, a spin-echo sequence with selective excitation of the lipid resonance was applied. To avoid noise due to relaxation, the echo time was minimized (4.5 ms) and a long repetition time of 3.5 s was chosen. During the 19.5-h measurement, an isotropic resolution of 80 μm was achieved. The images were quantified based on the total seed lipid content, determined using a Bruker minispec mq60.

Lipid Extraction

Total lipids were extracted from seeds as described (Chapman and Moore, 1993), except that seeds were flash frozen in liquid nitrogen and powdered with a mortar and pestle. Powdered seed material, while still frozen, was transferred to hot (70°C) isopropanol and incubated for 30 min to inactivate endogenous phospholipases. Chloroform was added at a ratio 2:1:0.45 (v/v/w) isopropanol:chloroform tissue to form a monophasic extraction solution that was incubated overnight at 4°C. Lipids were purified by two-phase partitioning with chloroform and 1 M KCl, and the organic layer was washed three times with 1 M KCl. Lipid samples were dried under N₂ and resuspended in chloroform and stored at -20°C under N₂ until MS or GC-MS analysis. Polar lipids were fractionated from TLEs by silica gel column chromatography in methanol (Supelco Discovery DSC-Si; 6 mL, 500-mg solid phase extraction cartridges) after eluting neutral lipids in two steps with hexane:diethyl ether at 4:1 and 1:1 by volume.

GC-MS Analysis of FA Composition

TLEs subjected to GC-MS analysis were dried under N₂ and resuspended in toluene. FA methyl esters (FAMES) were prepared via base-catalyzed transesterification essentially as described by Christie (1989). Briefly, 0.5 M sodium methoxide in anhydrous methanol (Sigma-Aldrich) was added to TLEs and maintained at 50°C for 10 min. After addition of acetic acid and water, FAMES were extracted into hexane.

FAMES were separated on an Agilent model 6890 GC with a DB-5 column and analyzed with a 5973 mass selective detector. A multiramp temperature program was applied for optimal separation with an initial 3-min initial hold at 150°C, increasing to 210°C at 10°C/min, increasing to 215°C at 0.8°C/min, increasing to 250°C at 5°C/min, increasing to 280°C at 15°C/min, and a final 2 min hold at 280°C.

Direct-Infusion ESI-MS

TLEs were analyzed by direct-infusion ESI-MS/MS (Bartz et al., 2007) on a Waters Micromass Quattro Ultima triple quadrupole mass spectrometer. Samples were evaporated to dryness and resuspended in 1:1 (v/v) chloroform:methanol plus 10 mM ammonium acetate for MS. TAGs were identified as ammonium adducts in positive ion mode with acyl composition determined through neutral loss fragmentation scans (collision energy 30) for individual acyl chains. TAGs were quantified in full scan mode. PCs were identified and quantified as hydrogen adducts in positive ion mode (collision energy 35) with a precursor loss of the phosphocholine head group (+184 m/z). PEs were identified and quantified as hydrogen adducts in positive ion mode (collision energy 30) with a neutral loss of the phosphoethanolamine head group (+141 m/z). Typical scanning conditions included a direct-infusion flow rate of 15 $\mu\text{L}/\text{min}$,

capillary voltage of 3.5 kV, cone voltage of 40 V, hexapole two voltage of 1.0 V, source/desolvation temperatures of 80/200°C, and cone/desolvation gas flows of 75/200 L/Hr. All solvents were optima grade from Thermo-Fisher Scientific.

Supplemental Data

The following materials are available in the online version of this article.

Supplemental Figure 1. Example Conversion of Raw MS Data to a Set of MS Images on an Absolute and Relative Scale.

Supplemental Figure 2. Fatty Acid Composition of Total Cottonseed Lipid Extracts.

Supplemental Table 1. Triacylglycerol Molecular Species Analyzed by MALDI-MSI.

Supplemental Table 2. Phosphatidylcholine Molecular Species Analyzed by MALDI-MSI.

Supplemental Table 3. Phosphatidylethanolamine Molecular Species Analyzed by MALDI-MSI.

Supplemental Table 4. Phosphatidic Acid Molecular Species Analyzed by MALDI-MSI.

Supplemental Movie 1. Video Reconstruction of the Distribution of Total Seed Lipid Content by Nuclear Magnetic Resonance.

ACKNOWLEDGMENTS

This research was supported in part by grants from Cotton Incorporated (Agreement 08-395) and from the U.S. Department of Energy (US-DOE), Office of Science, Biological and Environmental Research (DE-SC0000797) and Basic Energy Sciences (DE-FG02-05ER15647) to K.D.C. P.J.H. was supported through the University of North Texas Doctoral Fellowship program. The MSI measurements were conducted at the Ames Laboratory and supported by the US-DOE, Office of Basic Energy Sciences, Division of Chemical Sciences, Geosciences, and Biosciences through the Ames Laboratory. The Ames Laboratory is operated for the US-DOE by Iowa State University under Contract DE-AC02-07CH11358. We thank the Jannon L. Fuchs laboratory for access to the cryostat and assistance in preparing sections. We thank Duane Huggett for access to his Waters Micromass Quattro Ultima triple quadrupole mass spectrometer for direct-infusion ESI-MS/MS measurements.

AUTHOR CONTRIBUTIONS

K.D.C., Y.-J.L., P.J.H., P.B.N., V.S., and K.S. designed the research. A.R.K., P.B.N., P.J.H., J.F., L.B., E.L., and K.S. performed the research. P.J.H. wrote the lipidomics imaging software. All authors analyzed the data. P.J.H., K.D.C., and Y.-J.L. wrote the article with editorial assistance from others.

Received December 7, 2011; revised January 23, 2012; accepted February 1, 2012; published February 14, 2012.

REFERENCES

- Adams, R., Geissman, T.A., and Edwards, J.D. (1960). Gossypol, a pigment of cottonseed. *Chem. Rev.* **60**: 555–574.
- Bao, X., Katz, S., Pollard, M., and Ohlrogge, J. (2002). Carbocyclic fatty acids in plants: biochemical and molecular genetic characterization of cyclopropane fatty acid synthesis of *Sterculia foetida*. *Proc. Natl. Acad. Sci. USA* **99**: 7172–7177.

- Bartz, R., Li, W.-H., Venables, B., Zehmer, J.K., Roth, M.R., Welti, R., Anderson, R.G.W., Liu, P., and Chapman, K.D. (2007). Lipidomics reveals that adiposomes store ether lipids and mediate phospholipid traffic. *J. Lipid Res.* **48**: 837–847.
- Bates, P.D., Durrett, T.P., Ohlogge, J.B., and Pollard, M. (2009). Analysis of acyl fluxes through multiple pathways of triacylglycerol synthesis in developing soybean embryos. *Plant Physiol.* **150**: 55–72.
- Berry, K.A.Z., Li, B., Reynolds, S.D., Barkley, R.M., Gijón, M.A., Hankin, J.A., Henson, P.M., and Murphy, R.C. (2011). MALDI imaging MS of phospholipids in the mouse lung. *J. Lipid Res.* **52**: 1551–1560.
- Burrell, M., Earnshaw, C., and Clench, M. (2007). Imaging Matrix Assisted Laser Desorption Ionization Mass Spectrometry: A technique to map plant metabolites within tissues at high spatial resolution. *J. Exp. Bot.* **58**: 757–763.
- Cai, Y.-Z., Xing, J., Sun, M., and Corke, H. (2006). Rapid identification of betacyanins from *Amaranthus tricolor*, *Gomphrena globosa*, and *Hylocereus polyrhizus* by matrix-assisted laser desorption/ionization quadrupole ion trap time-of-flight mass spectrometry (MALDI-QIT-TOF MS). *J. Agric. Food Chem.* **54**: 6520–6526.
- Cha, S., Zhang, H., Ilarlan, H.I., Wurtele, E.S., Brachova, L., Nikolau, B.J., and Yeung, E.S. (2008). Direct profiling and imaging of plant metabolites in intact tissues by using colloidal graphite-assisted laser desorption ionization mass spectrometry. *Plant J.* **55**: 348–360.
- Chapman, K.D., and Moore, T.S., Jr. (1993). N-acylphosphatidylethanolamine synthesis in plants: Occurrence, molecular composition, and phospholipid origin. *Arch. Biochem. Biophys.* **301**: 21–33.
- Chapman, K.D., Neogi, P.B., Hake, K.D., Stawska, A.A., Speed, T.R., Cotter, M.Q., Garrett, D.C., Kerby, T., Richardson, C.D., Ayre, B.G., Ghosh, S., and Kinney, A.J. (2008). Reduced oil accumulation in cottonseeds transformed with a nonfunctional allele of a delta-12 fatty acid desaturase (FAD2). *Crop Sci.* **48**: 1470–1481.
- Chapman, K.D., and Ohlogge, J.B. (2012). Compartmentation of triacylglycerol accumulation in plants. *J. Biol. Chem.* **287**: 2288–2294.
- Chaurand, P., Cornett, D.S., Angel, P.M., and Caprioli, R.M. (2011). From whole-body sections down to cellular level, multiscale imaging of phospholipids by MALDI mass spectrometry. *Mol. Cell. Proteomics* **10**: O110.004259.
- Chen, Y., Allegood, J., Liu, Y., Wang, E., Cachón-Gonzalez, B., Cox, T.M., Merrill, A.H., Jr., and Sullards, M.C. (2008). Imaging MALDI mass spectrometry using an oscillating capillary nebulizer matrix coating system and its application to analysis of lipids in brain from a mouse model of Tay-Sachs/Sandhoff disease. *Anal. Chem.* **80**: 2780–2788.
- Christie, W.W. (1989). *Gas Chromatography and Lipids: A Practical Guide*. (Dundee, Scotland: Oily Press).
- Chughtai, K., and Heeren, R.M.A. (2010). Mass spectrometric imaging for biomedical tissue analysis. *Chem. Rev.* **110**: 3237–3277.
- Cornett, D.S., Reyzer, M.L., Chaurand, P., and Caprioli, R.M. (2007). MALDI imaging mass spectrometry: Molecular snapshots of biochemical systems. *Nat. Methods* **4**: 828–833.
- Dahlqvist, A., Ståhl, U., Lenman, M., Banas, A., Lee, M., Sandager, L., Ronne, H., and Stymne, S. (2000). Phospholipid:diacylglycerol acyltransferase: An enzyme that catalyzes the acyl-CoA-independent formation of triacylglycerol in yeast and plants. *Proc. Natl. Acad. Sci. USA* **97**: 6487–6492.
- Dowd, M.K. (2011). Cottonseed oil. In *Vegetable Oils in Food Technology: Composition, Properties and Uses*, 2nd ed, F.D. Gunstone, ed (Oxford, UK: Wiley-Blackwell), pp. 199–224.
- Dowd, M.K., Boykin, D.L., Meredith, W.R., Jr., Campbell, B.T., Bourland, F.M., Gannaway, J.R., Glass, K.M., and Zhang, J. (2010). Fatty acid profiles of cottonseed genotypes from the National Cotton Variety Trials. *J. Cotton Sci.* **14**: 64–73.
- Eggeling, C., Ringemann, C., Medda, R., Schwarzmann, G., Sandhoff, K., Polyakova, S., Belov, V.N., Hein, B., von Middendorff, C., Schönle, A., and Hell, S.W. (2009). Direct observation of the nanoscale dynamics of membrane lipids in a living cell. *Nature* **457**: 1159–1162.
- Emerson, B., Gidden, J., Lay, J.O., Jr., and Durham, B. (2010). A rapid separation technique for overcoming suppression of triacylglycerols by phosphatidylcholine using MALDI-TOF MS. *J. Lipid Res.* **51**: 2428–2434.
- Fuchs, B., Süß, R., and Schiller, J. (2010). An update of MALDI-TOF mass spectrometry in lipid research. *Prog. Lipid Res.* **49**: 450–475.
- Gidden, J., Liyanage, R., Durham, B., and Lay, J.O., Jr. (2007). Reducing fragmentation observed in the matrix-assisted laser desorption/ionization time-of-flight mass spectrometric analysis of triacylglycerols in vegetable oils. *Rapid Commun. Mass Spectrom.* **21**: 1951–1957.
- Han, X., and Gross, R.W. (2001). Quantitative analysis and molecular species fingerprinting of triacylglyceride molecular species directly from lipid extracts of biological samples by electrospray ionization tandem mass spectrometry. *Anal. Biochem.* **295**: 88–100.
- Han, X., and Gross, R.W. (2005). Shotgun lipidomics: Electrospray ionization mass spectrometric analysis and quantitation of cellular lipidomes directly from crude extracts of biological samples. *Mass Spectrom. Rev.* **24**: 367–412.
- Hankin, J.A., Barkley, R.M., and Murphy, R.C. (2007). Sublimation as a method of matrix application for mass spectrometric imaging. *J. Am. Soc. Mass Spectrom.* **18**: 1646–1652.
- Hankin, J.A., and Murphy, R.C. (2010). Relationship between MALDI IMS intensity and measured quantity of selected phospholipids in rat brain sections. *Anal. Chem.* **82**: 8476–8484.
- Hedin, P.A., Parrott, W.L., and Jenkins, J.N. (1992). Relationships of glands, cotton square terpenoid aldehydes, and other allelochemicals to larval growth of *Heliothis virescens* (Lepidoptera: Noctuidae). *J. Econ. Entomol.* **85**: 359–364.
- Horn, P., Neogi, P., Tombokan, X., Ghosh, S., Campbell, B., and Chapman, K. (2011b). Simultaneous quantification of oil and protein in cottonseed by low-field time-domain nuclear magnetic resonance. *J. Am. Oil Chem. Soc.* **88**: 1521–1529.
- Horn, P.J., and Chapman, K.D. (2011). Organellar lipidomics. *Plant Signal. Behav.* **6**: 1594–1596.
- Horn, P.J., Ledbetter, N.R., James, C.N., Hoffman, W.D., Case, C.R., Verbeck, G.F., and Chapman, K.D. (2011a). Visualization of lipid droplet composition by direct organelle mass spectrometry. *J. Biol. Chem.* **286**: 3298–3306.
- Hu, Q., Noll, R.J., Li, H., Makarov, A., Hardman, M., and Graham Cooks, R. (2005). The Orbitrap: A new mass spectrometer. *J. Mass Spectrom.* **40**: 430–443.
- Jones, L.A., and King, C.C. (1996). Cottonseed oil. In *Bailey's Industrial Oil and Fat Products*, Y. Hui, ed (New York: John Wiley & Sons), pp. 159–240.
- Jun, J.H., Song, Z., Liu, Z., Nikolau, B.J., Yeung, E.S., and Lee, Y.J. (2010). High-spatial and high-mass resolution imaging of surface metabolites of *Arabidopsis thaliana* by laser desorption-ionization mass spectrometry using colloidal silver. *Anal. Chem.* **82**: 3255–3265.
- Kaspar, S., Peukert, M., Svatos, A., Matros, A., and Mock, H.-P. (2011). MALDI-imaging mass spectrometry - An emerging technique in plant biology. *Proteomics* **11**: 1840–1850.
- Katagiri, T., Ishiyama, K., Kato, T., Tabata, S., Kobayashi, M., and Shinozaki, K. (2005). An important role of phosphatidic acid in ABA signaling during germination in *Arabidopsis thaliana*. *Plant J.* **43**: 107–117.
- Koestler, M., Kirsch, D., Hester, A., Leisner, A., Guenther, S., and Spengler, B. (2008). A high-resolution scanning microprobe matrix-assisted laser desorption/ionization ion source for imaging analysis on

- an ion trap/Fourier transform ion cyclotron resonance mass spectrometer. *Rapid Commun. Mass Spectrom.* **22**: 3275–3285.
- Lee, Y.J., Perdian, D.C., Song, Z., Yeung, E., and Nikolau, B.** (2012). Use of mass-spectrometry for imaging metabolites in plants. *Plant J.*, in press.
- Lisa, M., and Holcapek, M.** (2008). Triacylglycerols profiling in plant oils important in food industry, dietetics and cosmetics using high-performance liquid chromatography-atmospheric pressure chemical ionization mass spectrometry. *J. Chromatogr. A* **1198-1199**: 115–130.
- Liu, Q., Singh, S., Chapman, K., and Green, A.** (2009). Bridging traditional and molecular genetics in modifying cottonseed oil. In *Genetics and Genomics of Cotton*, A.H. Paterson, ed (New York: Springer), pp. 1–30.
- Lu, C., Xin, Z., Ren, Z., Miquel, M., and Browse, J.** (2009). An enzyme regulating triacylglycerol composition is encoded by the ROD1 gene of *Arabidopsis*. *Proc. Natl. Acad. Sci. USA* **106**: 18837–18842.
- Murphy, R.C., Hankin, J.A., and Barkley, R.M.** (2009). Imaging of lipid species by MALDI mass spectrometry. *J. Lipid Res.* **50** (suppl.): S317–S322.
- Neuberger, T., Sreenivasulu, N., Rokitta, M., Rolletschek, H., Göbel, C., Ruten, T., Radchuk, V., Feussner, I., Wobus, U., Jakob, P., Webb, A., and Borisjuk, L.** (2008). Quantitative imaging of oil storage in developing crop seeds. *Plant Biotechnol. J.* **6**: 31–45.
- Obert, J.C., Hughes, D., Sorenson, W.R., McCann, M., and Ridley, W.P.** (2007). A quantitative method for the determination of cyclopropanoid fatty acids in cottonseed, cottonseed meal, and cottonseed oil (*Gossypium hirsutum*) by high-performance liquid chromatography. *J. Agric. Food Chem.* **55**: 2062–2067.
- Perdian, D.C., and Lee, Y.J.** (2010). Imaging MS methodology for more chemical information in less data acquisition time utilizing a hybrid linear ion trap-orbitrap mass spectrometer. *Anal. Chem.* **82**: 9393–9400.
- Qiao, H., Spicer, V., and Ens, W.** (2008). The effect of laser profile, fluence, and spot size on sensitivity in orthogonal-injection matrix-assisted laser desorption/ionization time-of-flight mass spectrometry. *Rapid Commun. Mass Spectrom.* **22**: 2779–2790.
- Schaub, T.M., Hendrickson, C.L., Horning, S., Quinn, J.P., Senko, M.W., and Marshall, A.G.** (2008). High-performance mass spectrometry: Fourier transform ion cyclotron resonance at 14.5 Tesla. *Anal. Chem.* **80**: 3985–3990.
- Schmelzer, K., Fahy, E., Subramaniam, S., and Dennis, E.A.** (2007). The lipid maps initiative in lipidomics. In *Methods in Enzymology*, H.A. Brown, ed (San Diego, CA: Academic Press), pp. 171–183.
- Schmid, K.M., and Patterson, G.W.** (1988). Distribution of cyclopropanoid fatty acids in malvaceous plant parts. *Phytochemistry* **27**: 2831–2834.
- Sperling, P., Linscheid, M., Stöcker, S., Mühlbach, H.P., and Heinz, E.** (1993). In vivo desaturation of cis-delta 9-monounsaturated to cis-delta 9,12-diunsaturated alkenylether glycerolipids. *J. Biol. Chem.* **268**: 26935–26940.
- Stipanovic, R.D., Bell, A.A., and Benedict, C.R.** (1999). Cotton pest resistance: The role of pigment gland constituent. In *Biologically Active Natural Products: Agrochemicals*, H.G. Cutler and S.J. Cutler, eds (Boca Raton, FL: CRC Press), pp. 211–220.
- Strupat, K., Kovtoun, V., Bui, H., Viner, R., Stafford, G., and Horning, S.** (2009). MALDI produced ions inspected with a linear ion trap-Orbitrap hybrid mass analyzer. *J. Am. Soc. Mass Spectrom.* **20**: 1451–1463.
- Stymne, S., and Stobart, A.** (1987). Triacylglycerol biosynthesis. In *The Biochemistry of Plants: A Comprehensive Treatise*, P. Stumpf, ed (New York: Academic Press), pp. 175–214.
- Stymne, S., and Stobart, A.K.** (1984). Evidence for the reversibility of the acyl-CoA:lysophosphatidylcholine acyltransferase in microsomal preparations from developing safflower (*Carthamus tinctorius* L.) cotyledons and rat liver. *Biochem. J.* **223**: 305–314.
- Sunilkumar, G., Campbell, L.M., Puckhaber, L., Stipanovic, R.D., and Rathore, K.S.** (2006). Engineering cottonseed for use in human nutrition by tissue-specific reduction of toxic gossypol. *Proc. Natl. Acad. Sci. USA* **103**: 18054–18059.
- Suzuki, T., Midonoya, H., and Shioi, Y.** (2009). Analysis of chlorophylls and their derivatives by matrix-assisted laser desorption/ionization-time-of-flight mass spectrometry. *Anal. Biochem.* **390**: 57–62.
- Testerink, C., and Munnik, T.** (2005). Phosphatidic acid: A multifunctional stress signaling lipid in plants. *Trends Plant Sci.* **10**: 368–375.
- Verleyen, T., Forcades, M., Verhe, R., Dewettinck, K., Huyghebaert, A., and De Greyt, W.** (2002). Analysis of free and esterified sterols in vegetable oils. *J. Am. Oil Chem. Soc.* **79**: 117–122.
- Vieler, A., Wilhelm, C., Goss, R., Süß, R., and Schiller, J.** (2007). The lipid composition of the unicellular green alga *Chlamydomonas reinhardtii* and the diatom *Cyclotella meneghiniana* investigated by MALDI-TOF MS and TLC. *Chem. Phys. Lipids* **150**: 143–155.
- Vrkoslav, V., Muck, A., Cvacka, J., and Svatos, A.** (2010). MALDI imaging of neutral cuticular lipids in insects and plants. *J. Am. Soc. Mass Spectrom.* **21**: 220–231.
- Wang, X., Devaiah, S.P., Zhang, W., and Welti, R.** (2006). Signaling functions of phosphatidic acid. *Prog. Lipid Res.* **45**: 250–278.
- Welti, R., Shah, J., Li, W., Li, M., Chen, J., Burke, J.J., Fauconnier, M.-L., Chapman, K., Chye, M.L., and Wang, X.** (2007). Plant lipidomics: Discerning biological function by profiling plant complex lipids using mass spectrometry. *Front. Biosci.* **12**: 2494–2506.
- Wessels, J.T., Yamauchi, K., Hoffman, R.M., and Wouters, F.S.** (2010). Advances in cellular, subcellular, and nanoscale imaging in vitro and in vivo. *Cytometry A* **77**: 667–676.
- Wiesman, Z., and Chapagain, B.P.** (2009). Determination of fatty acid profiles and TAGs in vegetable oils by MALDI-TOF/MS fingerprinting. *Methods Mol. Biol.* **579**: 315–336.
- Yunusova, S.G., Gusakova, S.D., and Umarov, A.U.** (1982). Stereospecific analysis of the triacylglycerols of cottonseed oil. *Chem. Nat. Compd.* **18**: 396–399.
- Zabrouskov, V., Al-Saad, K.A., Siems, W.F., Hill, H.H., Jr., and Knowles, N.R.** (2001). Analysis of plant phosphatidylcholines by matrix-assisted laser desorption/ionization time-of-flight mass spectrometry. *Rapid Commun. Mass Spectrom.* **15**: 935–940.
- Zaima, N., Goto-Inoue, N., Hayasaka, T., and Setou, M.** (2010). Application of imaging mass spectrometry for the analysis of *Oryza sativa* rice. *Rapid Commun. Mass Spectrom.* **24**: 2723–2729.
- Zhang, H., Cha, S., and Yeung, E.S.** (2007). Colloidal graphite-assisted laser desorption/ionization MS and MS(n) of small molecules. 2. Direct profiling and MS imaging of small metabolites from fruits. *Anal. Chem.* **79**: 6575–6584.